



**HAL**  
open science

# Residence time distribution on flow characterisation of multichannel systems: Modelling and experimentation

Xiaofeng Guo, Yilin Fan, Lingai Luo

► **To cite this version:**

Xiaofeng Guo, Yilin Fan, Lingai Luo. Residence time distribution on flow characterisation of multichannel systems: Modelling and experimentation. *Experimental Thermal and Fluid Science*, 2018, 99, pp.407 - 419. 10.1016/j.expthermflusci.2018.08.016 . hal-01890617

**HAL Id: hal-01890617**

**<https://hal.science/hal-01890617>**

Submitted on 4 Nov 2020

**HAL** is a multi-disciplinary open access archive for the deposit and dissemination of scientific research documents, whether they are published or not. The documents may come from teaching and research institutions in France or abroad, or from public or private research centers.

L'archive ouverte pluridisciplinaire **HAL**, est destinée au dépôt et à la diffusion de documents scientifiques de niveau recherche, publiés ou non, émanant des établissements d'enseignement et de recherche français ou étrangers, des laboratoires publics ou privés.



## Residence time distribution on flow characterisation of multichannel systems: Modelling and experimentation



Xiaofeng Guo<sup>a,\*</sup>, Yilin Fan<sup>b</sup>, Lingai Luo<sup>b</sup>

<sup>a</sup> ESIEE Paris, Université Paris Est, LIED UMR CNRS 8236, 2 boulevard Blaise Pascal – Cité Descartes, 93162 Noisy Le Grand, France

<sup>b</sup> Laboratoire de Thermique et Energie de Nantes (LTEN), UMR CNRS 6607, Université de Nantes, Rue Christian Pauc, BP 50609, 44306 Nantes Cedex 03, France

### ARTICLE INFO

#### Keywords:

Residence Time Distribution (RTD)  
Non-intrusive measurement  
Flow distribution  
Multichannel device

### ABSTRACT

Residence Time Distribution (RTD) is a frequently used tool in conventional process equipment and it provides internal flow characterisation by simple tracer tests. In this paper, we explore the feasibility of using RTD to identify fluid distribution uniformity in millimetric multichannel devices. Both theoretical modelling and experimental implementation are conducted to 16-channel systems. Theoretical modelling confirms the effectiveness of non-intrusive RTD measurements in evaluating flowrate distribution uniformity. Different influencing factors, such as channel corrosion, blockage, distributor structure, channel length or width variation, etc., can be reflected by RTD response curve. The experimental setup consists of a lab-developed RTD test platform coupling a fast camera and two miniflowcells capable to quantify rapid tracer concentration evolution through carbon ink visualization. The platform is particularly powerful for very narrow RTD measurement with residence time down to 1 s. With the platform, we investigate the RTD characteristics of a multichannel device under several flow conditions. Model correlation of the experimental data gives valuable information such as fluid distribution, plug-flow ratio and perfectly mixed volume.

### 1. Introduction

Significant progresses in Process Intensification [1,2] have been seen in last decades. They are characterised by compact size and enhanced performances in fluids mixing, heat transfer as well as chemical syntheses yields. However, industrial applications usually require large production rate which in general means high throughput, a weak point for most micro- or mini-devices. Numbering-up process [3–8] is then applied, in the form of 2D or 3D multichannel/layer systems or modular reconfigurable devices. Particularly for multichannel systems, the parallelisation of a large number of flow/mixing/reaction paths helps achieve industrial-level production.

Fluid distribution uniformity in multichannel devices is considered as a key issue to achieve high global performances. A number of studies in the literature have confirmed the influence of flowrate distribution in multichannel heat exchangers [9], mixers [10,11] and chemical reactors [12–14]. One of the existing difficulties in the evaluation of fluid distribution influence lies in the identification of flow distribution uniformity (in terms of flowrate). Non-intrusive measurements are necessary in case of non-transparent devices for which flow visualisation test is not applicable. This paper introduces our modelling and experimentation works on the development of a non-intrusive method

based on Residence Time Distribution (RTD) characterization and its application to multichannel devices for their fluid flow distribution diagnostic.

#### 1.1. Previous studies

Parallel millimetric channels can be configured to provide multiple functionalities including heat exchange, mixing and chemical reaction. Our previous studies [10,15,16] on a 16-channel device have demonstrated rapid mixing effect (with micromixing time down to 10 ms) and compact heat exchange property (with the overall heat transfer coefficient being in the range of 2000–5000 W m<sup>-2</sup> K<sup>-1</sup>). All these performances are thanks to a special tree-like structure that serves as fluid distributor and collector. By using such a nature-inspired manifold, the flow distribution non-uniformity is estimated to be lower than 10% under test flow conditions.

However, once channel flowrates differ among channels (non-uniform distribution, or maldistribution), the global performance is expected to degrade in most cases. Regarding micromixing and chemical reaction, uneven fluid distribution can result in unbalanced reagents composition thus totally different reaction kinetics. Shown in Fig. 1 is the link between fluid residence time and micromixing time, previously

\* Corresponding author at: ESIEE Paris, Department SEN, 2 bd Blaise Pascal BP99, 93162, Noisy Le Grand Cedex, France.

E-mail address: [xiaofeng.guo@esiee.fr](mailto:xiaofeng.guo@esiee.fr) (X. Guo).

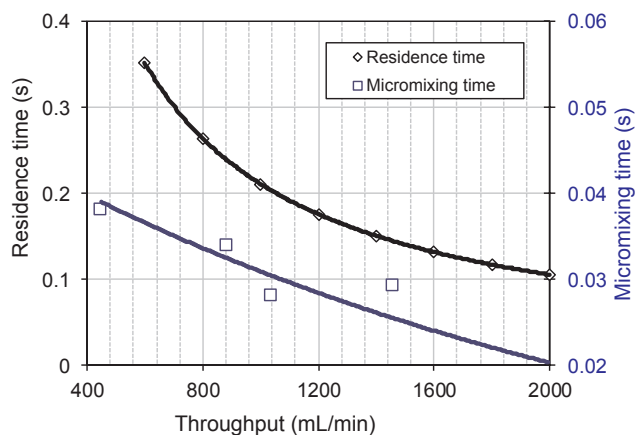


Fig. 1. The link between residence time and micromixing time in a static micromixer.

measured inside the 16-channel device [16]. It can be seen that, without a mechanical aided mixing, the two time variables are closely related and dependent on the channel flowrate. In other words, uneven flowrate distribution in a multichannel device may result in different micromixing time among channels, implying less controllable syntheses and heterogeneous final products.

In some specific cases, uneven fluid distribution may have positive influence on mixing. As in the study of Su et al. 2015 [17] on a multichannel zigzag microreactor, if the overall flowrate is kept the same, partial channel blockage may enhance mixing since more fluid perturbation happens in non-blocked channels with higher flowrates. In case of gross maldistribution, stronger fluid impingements in collectors also enhance the mixing process. However, the above conclusions only are applicable only under two conditions: (i) the mixing should be slow so that it does not finish before going into the collector zone, and (ii) a higher pressure loss with the same overall flowrate guaranteed by a pump. Our study focuses on straight pipes that will be used for rapid mixing/reaction applications and we suppose that they all require uniform fluid distribution for better performance.

As the influence of flow distribution uniformity on various performances of multichannel device is significant, the perfect reproduction of single pipe performances is strongly expected during numbering-up process. The ability to predict or identify the fluid distribution uniformity in a multichannel device by a non-intrusive experimental method is hence helpful.

### 1.2. Existing methods in fluid distribution identification

Main methodologies in the diagnostic of fluid distribution in multichannel devices can be categorized by numerical simulation and flow visualization. The use of non-intrusive tool such as RTD should be much helpful yet not sufficiently advanced in the literature.

CFD (Computational Fluid Dynamics) simulation is an interesting and practical tool intensively used for the prediction or characterization of hydrodynamic and/or thermal properties of multichannel devices, sometimes with the purpose of structural optimization. A number of studies using CFD tools have been reported in the literature [18–21]. Nevertheless, it should be noted that current CFD techniques still have some difficulties in correctly describing turbulent flows, vortex or curvature flows and multi-phase flows. Moreover, CFD results need to be validated by experimental measurements.

Besides numerical methods, existing experimental techniques for the evaluation of fluid distribution are limited to visualizations by color, pH indicator or fluorescence tracers [22–24]. Other intrusive experimental methods such as Hot Wire Probe (HWP), Doppler Ultrasonic Velocimetry (DUV) are compared by Boutin et al. [25]. But the

above-listed techniques give only single point measurement other than detailed flow distribution information. Concentration measurement using salt as tracer [26] can be an effective solution for conventional devices. When comes to millimetric device that have short residence time, this method is limited by the sampling rate of conductometer. PIV (Particle Image Velocimetry) [25,27] and LIF (Laser Induced Fluorescence) [28] measurements provide quantitative velocity distribution inside certain flow configurations, but under specific conditions. First, the visualization is usually limited to simple or single-pipe devices but not adapted to 3D complex configurations. Second, PIV or LIF measurements require that the studied structure being transparent [28] in accordance with the wave length of the laser source.

The development of a non-intrusive tool for fluid distribution characterization based on inlet-outlet detection should be more practical for the identification of general multichannel flow systems. To the authors' knowledge, very few studies in the literature addressed the fluid distribution issue by RTD tool. Detailed RTD analyses merit being involved to explore the relationship between RTD characters and the flow distribution uniformity.

### 1.3. RTD and its application

Non-intrusive tracer test has been widely used in process engineering except for quantitative fluid distribution determination. After the pioneer work of MacMullin and Weber in 1935 [29] and several classical interpretations of RTD by Danckwerts in 1953 [30], extensive applications have been found in the field of chemical engineering. Macro-mixing and hydraulic characteristics of a process device could be reflected through examining the RTD curve [31]. RTD has also been used to predict the chemical reaction conversions by combining chemical kinetics and RTD analysis [32] or to determine optimal design parameters of tubular reactors [33]. Besides conventional RTD models for CSTRs (Continuous Stirred Tank Reactor) and PFRs (Plug Flow Reactor), some recent applications in multichannel systems in the aim of flow and mixing characterisation attracts some attention too [34–38]. In particular, recent works by Wibel et al. [39] investigated the impact of inlet/outlet volumes and uneven flow distribution on the RTD characters of micro devices consisting of an array of parallel microchannel, by both CFD simulation and experimental characterization.

For miniaturized process devices, one of the challenges to conduct a RTD analysis lies in the choice of tracer and its detection instrument. Especially for non-transparent devices, particle or dye visualisation [40] are generally impossible. Dong et al. [41] developed single channel Ultrasonic Microreactor and studied the effect of ultrasonic field on the mixing and RTD. The mechanism of ultrasonic induced cavitation (bubbles sizing 100–200  $\mu\text{m}$ ) intensifies radial mixing and reduces axial dispersion within the reactor channel (characteristic dimension from 250  $\mu\text{m}$  to 1 mm). Their RTD measurements are based on UV-Vis spectrometer tracing 5 g/L uranine solution. This technique is more adapted to long residence time (around 100 s in their case). For very narrow RTD measurement, the spectrometer's sampling time may limit its application. In conclusion, quantitative fluid distribution (in terms of flowrate) determination by an easy-to-use RTD measurement is still lacking. Moreover, due to short residence time and narrow RTD curve of millimetric devices, traditional methods like conductivity measurement using salt as tracer [26], become limited by sampling rates. Developing a rapid RTD detection platform applicable to micro- or mini-fluidic devices is then of practical significance.

### 1.4. Current study

The main contribution of this study is to demonstrate the utility of RTD tool for the characterization of fluid distribution uniformity in multichannel devices. The study begins with the modelling of the RTD behavior of multichannel device with non-uniform distribution assumptions; then, an experimental platform applied to a previously

developed mini-reactor is explained in detail.

The modelling and experimentation are conducted taking a 16-channel fluidic system as example. In the modelling part, axial dispersion RTD representation is firstly established in each channel, according to its flowrate and other geometrical parameters. Then, supposing flowrate deviation among the 16 channels, we obtain the global RTD of the whole device. The comparison between a perfect, homogeneous distribution case and a non-uniform distribution case will confirm the feasibility of flow distribution diagnostic through a non-intrusive RTD injection-response measurement. For the experimentation part, a tracer injection-detection platform with the aim of identifying short residence time and narrow RTD curves is introduced and explained in detail. The basic principle is instantaneous tracer concentration determination by using fast camera and image analysis. We confirm the feasibility of using the developed platform to identify the RTD of our device with throughput time down to 1 s. In general, this tracer test platform can be easily adapted to other micro- or mini-fluidic systems regardless of its residence time being long or short.

It worth noting that the modelling and experimental parts are not meant for results validation but to show *independently* the role of RTD study for distribution uniformity. We aim to show large RTD deviation due to uneven fluid distribution by making specific assumptions in the modelling process. The distributor and collector parts are not considered in the model. In the experimental part, however, we use our previously developed reactor whose fluid distribution uniformity is already guaranteed thanks to tree-like bifurcation distributor and collectors.

The rest of the paper is organized as follows: (i) the RTD modelling of multichannel fluid system, (ii) detail of the development of a rapid RTD measurement system, and (iii) discussions on the overall methodology.

## 2. RTD modelling of a multichannel system

The procedure of the RTD modelling is as follows: (i) single pipe flow modelling under fully developed laminar condition using Dispersive Plug Flow (DPF) model; (ii) determination of flowrates in each channel in a multichannel device under different conditions, and (iii) composition of all single channel RTD signals to obtain the global RTD curve. Non-uniform flow distribution originated from different factors (channel length variation, width difference, distributor/collector design, etc.) is considered. The influence of channel flowrate deviation on the global RTD curve is modelled. However, fluid distribution and collection are not considered in the model.

Pipe dispersive flow is considered to model each channel before constructing the global RTD model for a multichannel system. The following general hypotheses are used:

- (i) Fully developed laminar flow;
- (ii) Circular cross section channels, pipe flow;
- (iii) Only spatial dispersion (shear force induced diffusion) caused by velocity gradient (hence concentration gradient) is considered, turbulence caused diffusion does not exist.

### 2.1. Multichannel RTD modelling – general approach

In a multichannel system, the tracer concentration evolution under fully developed laminar flow in channel  $i$  can be expressed by DPF model, given by Eq. (1) [37]. The single channel RTD is a function of Peclet number  $Pe$  and dimensionless time  $t/\tau_m$ .

$$E_i(t) = \sqrt{\frac{Pe_i + 1}{4\pi(t/\tau_{m,i})^3}} \exp\left(\frac{-(Pe_i + 1)(1-t/\tau_{m,i})^2}{4t/\tau_{m,i}}\right) \quad (1)$$

where  $E_i(t)$  represents the RTD response in channel  $i$ ,  $t$  time of pipe flow (s) and  $\tau_m$  the mean pass-through time (s).

The dimensionless  $Pe$  number is given by:

$$Pe = \frac{uL}{D} \quad (2)$$

where  $u$  is the average velocity inside pipe ( $\text{m s}^{-1}$ ),  $L$  length of the pipe (m) and  $D$  the dispersion coefficient, ( $\text{m}^2 \text{s}^{-1}$ ), obtained with Taylor correlation [31]:

$$D = D_m + \frac{u^2 d^2}{D_m} \quad (3)$$

$D_m$  is the molecular diffusion of water,  $u$  the velocity of flow and  $d$  the channel diameter. In our case, the molecular diffusion is negligible compared with the axial dispersion.

Then the global RTD could be calculated using Eq. (4), by combining all individual RTD curves considering individual channel flowrates as a weighting factor.

$$E(t) = \frac{1}{Q} \sum_{i=1}^n Q_i E_i(t) \quad (4)$$

where  $Q$  is the total volume flowrate, and  $Q_i$  the individual volume flowrate in channel  $i$ .

In a single pipe, hydraulic relation associates parameters including pressure loss ( $\Delta P_i$ ), geometry ( $d$  and  $L$ ) and flowrate ( $Q_i$ ), using  $\Delta P_i = f(d_i, L_i, Q_i)$ . Under laminar regime, the pressure loss for pipe flow is governed by Hagen-Poiseuille law given by Eq. (5). The equation, applied to different channels, provides basic calculation for flowrate distribution among different channels.

$$\Delta P_i = \frac{128\mu L_i Q_i}{\pi d_i^4} \quad (5)$$

Until this step, a RTD analysis can be constructed to a multichannel device, taking into account different cases such as channel length variation, diameter difference, gross fluid maldistribution due to distributor design, block of one or several channels, corrosion of one or several channels, etc.

### 2.2. Flowrate distribution coupling

Based on the multichannel RTD model, two categories of cases are studied. The first category is passage-to-passage maldistribution, induced by variation of length, diameter, corrosion or blockage. The inlet distributor and the outlet collector are supposed to be perfect so that they provide equal pressure loss ( $\Delta P_i$ ) to every channel. The second category is named *gross maldistribution* case due to improper distributor/collector design. In this case, channel geometric parameters including diameter and length are identical. However, the channel flowrate may differ from one pipe to another.

The two categories will be treated separately. For the passage-to-passage maldistribution category, the channel flowrates are calculated based on the pressure balance while for the gross maldistribution category, the flowrate distribution is predefined. Once individual flowrates obtained, the global RTD model is constructed by combining all individual RTD curves.

#### 2.2.1. Case of length variation

Modelling of length-varied multichannel RTD is based on the following hypotheses:

- (i) Varied channel lengths  $L_i$ ;
- (ii) Fixed total flowrate  $Q$ , internal volume  $V$  as well as identical channel diameter  $d$ ;
- (iii) Identical pressure loss  $\Delta P$  for every channel;

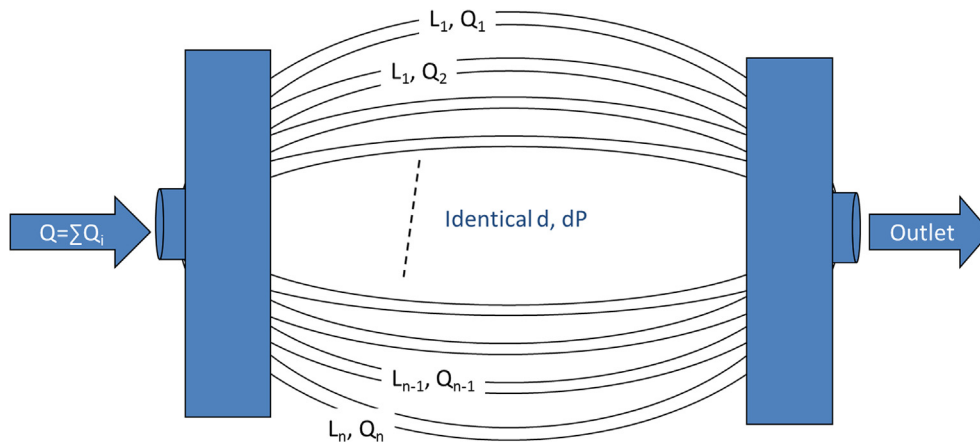


Fig. 2. Multichannel RTD model, case of length variation.

$$\Delta P_1 = \Delta P_2 = \dots = \Delta P_i = \Delta P$$

$$\Delta P = \frac{128\mu}{\pi d^4} \sum_{i=1}^n \frac{1}{L_i} Q \quad (6)$$

(iv) Based on the previously determined pressure loss, individual channel flowrate ( $Q_i$ ) is calculated as:

$$Q_i = \frac{\pi d^4}{128\mu L_i} \Delta P \quad (7)$$

(v) Tracer (Dirac impulse) amounts injected into channels are proportional to flowrate ( $Q_i/Q$ );

The model assumptions with the length-varied geometry are illustrated in Fig. 2. Practically, the variance of channel length  $L_i$  is usually a result of inappropriate design or imprecise fabrication of one or several channels during numbering-up process.

### 2.2.2. Case of diameter variation

In this case, all other hypotheses are the same as the previous one (Section 2.2.1), except for the first two:

- (i) Varied diameter  $d_i$ , identical channel length  $L$ ;
- (ii) Fixed total flowrate  $Q$ , and volume  $V$ ;

Eqs. (6) and (7) in this case shall be modified as Eq. (8) for the determination of pressure loss and then Eq. (9) to obtain individual channel flowrate:

$$\Delta P = \frac{128L\mu}{\pi} \sum_{i=1}^n \frac{Q}{d_i^4} \quad (8)$$

$$Q_i = \frac{\pi d_i^4}{128\mu L} \Delta P \quad (9)$$

The model assumptions with diameter varied geometry are illustrated in Fig. 3. Under practical situations, the variation of diameter  $d_i$  may come from (i) total blockage of one or several channels; (ii) deterioration enlarging the diameter; (iii) partial blockage of channel because of fouling; and (iv) inappropriate design or fabrication of multiple channels during the numbering-up process. It worth noting that in the total blockage situation, the model considers reduced number of channels and keeps the same pressure drop in the effective channels.

### 2.2.3. Case of gross maldistribution

The gross maldistribution is mainly due to improper design of distributor/collector and one of them is the ladder network as shown in

the upper left corner of Fig. 4. The modelling process is based on hypotheses below:

- (i) Identical  $d$  and  $L$  for all pipes;
- (ii) Fixed  $Q$ ,  $V$ ;
- (iii) Channel flowrate  $Q_i$  is predefined in the following modelling;
- (iv) Channel pressure loss ( $\Delta P_i$ ) is no longer identical;
- (v) Tracer (Dirac impulse) amounts injected into channels are proportional to flowrate ( $Q_i/Q$ );

## 2.3. Results and discussion

The modelling is implemented in Matlab© [42] environment. The following discussions are based on both qualitative comparisons and quantitative statistical analyses. Under non-uniform flow distribution situation, individual RTD curves in pipe  $i$  might vary from one to another. After being put together, the shape and spreading character of the global RTD curve can be observed, which clearly differ from that under uniform distribution condition. Time location of concentration peak can be different too. Moreover, comparison of curve variance ( $\sigma^2$ ) gives quantitative deviation information between non-uniform and uniform distribution conditions.

### 2.3.1. Case of length variation

The first case study is a 16-channel system with identical diameter of 1 mm, but length varied from 0.44 to 1.94 m, following a parabolic curve as shown in Fig. 5(a). The case of identical length of 1 m, which represents the same total volume (channel only, 12.6 mL) as the varied one, is also modelled for comparison. The pass-through time for both cases is the same, i.e., 12.6 s under a flowrate of 60 mL·min<sup>-1</sup>.

Shown in Fig. 5(b) are RTD curves in all 16 channels for the varied-length case. For channels numbering from 5 to 11, their concentration peaks arrive within 10 s. The RTD peaks in longer channels, however, appear much later than the average pass-through time 12.5 s. Corresponding  $Pe$  number ranges from 2.3 for shortest channels in the middle to 17.1 for longest ones at the side.

The global inlet-outlet RTD curve, both in cases of varied- and identical length, are shown in Fig. 5(c). Two features can be observed in this figure: the peak arrival time and the tailing effect. Firstly, it can be observed that under uneven distribution case, peak concentration arrives at around 2.5 s. Compared with the value of 6.5 s for identical channel case, the varied-length concentration peak arrives much earlier. A large number of tracers follows higher flowrates in short channels. Secondly, length-varied multichannel device holds a tailing effect. The outlet tracer detection can last much longer than the average pass-through time; while for the uniform distribution case, no tracer can be detected after 30 s. This can be explained by much lower  $Pe$  number in

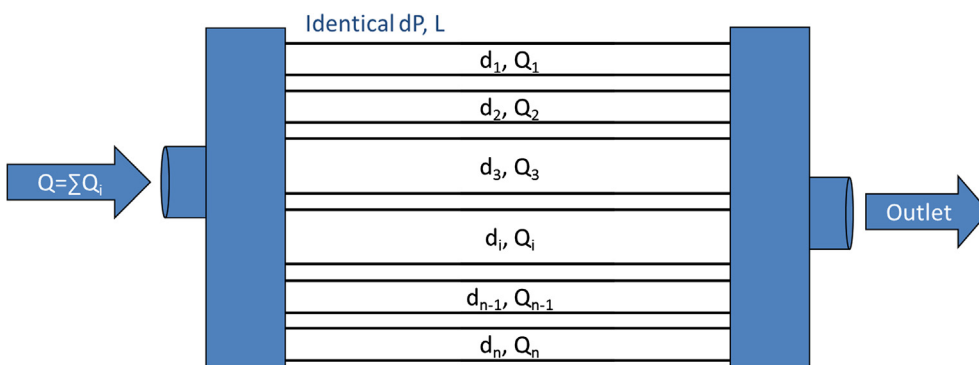


Fig. 3. Multi-channel RTD model, case of diameter variation.

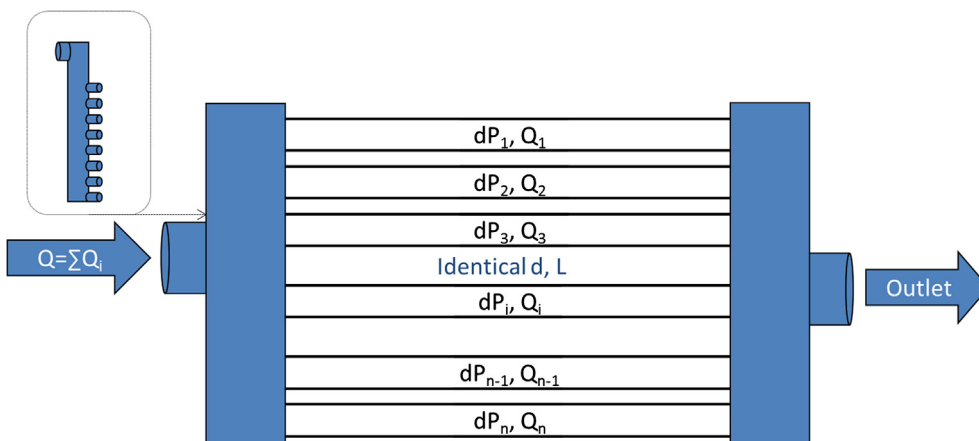


Fig. 4. Multi-channel RTD model, case of gross maldistribution.

longer channels where tracers spend more time to traverse such paths.

To quantitatively evaluate influence of length variation on the spreading character of RTD curve, the second moment of tracer curve, the variance ( $\sigma^2$ ), is analysed. Shown in Fig. 5(d) are RTD curves of multichannel device, with different degree of flowrate deviation ( $Q_{dv}$ ) due to length variation. Note that the parameter  $Q_{dv}$ , as shown in Eq. (10), is defined as the maximal difference of flowrate among channels devised by the average flowrate, [-]: A  $Q_{dv}$  value of zero means perfect distribution.

$$Q_{dv} = \frac{Q_{i,max} - Q_{i,min}}{Q_{mean}} \quad (10)$$

We may observe from the RTD curves that the higher the flowrate deviation ( $Q_{dv}$ ), the higher the order of magnitude of the RTD variance ( $\sigma^2$ ). For the worst case, i.e., flowrate deviation of 78% corresponds to a variance of  $120 \text{ s}^2$  in  $E(t)$  curve. While for the ideal uniform case, the minimum value of variance is  $38 \text{ s}^2$ . RTD is quantitatively shown to be more expanded with existence of distribution non-uniformity, meaning that the residence times for different portions of reactants are largely varied.

Absolute value of variance, however, depends highly on the flow conditions as flowrate, channel number, etc. Once the above parameters are fixed, the variance of ideal RTD curve is fixed. Further RTD tests under the same condition, if showing a higher variance, means the departure from the uniform condition.

### 2.3.2. Case of diameter variation

In case of one or several channels being blocked or enlarged due to corrosion, the modelling considers diameter variation. The total volume  $V$  reduces while the global flowrate  $Q$  is kept the same by a pumping system.

Shown in Fig. 6(a) is the comparison of obtained  $E(t)$  curves

between a case of 4 channels in 16 being blocked and another case without blockage. First of all, earlier tracer peaks at the outlet can be observed in the blockage case (3 s instead of 6 s). This means shorter pass-through time in case of channel blockage since part of the total volume becomes dead volume. Secondly, in contrary with the length variation case, no tailing effect is observed when 4 channels are blocked. Pelect number is increased due to dead volume and the flow becomes closer to piston flow.

Simplified corrosion case can also be modeled by supposing enlarged diameter to one or several channels. Fig. 6(b) shows two RTD curves comparing in one case 20% enlarged diameter for 4 channels and the other under normal situation. The 4 enlarged channels result in expanded  $E(t)$  curve, meaning different  $Pe$  numbers in normal and enlarged channels. More precisely, extra volume in corroded channels results in smaller  $Pe$  number thus more diffusive flow. The global RTD curve in this case is then more expanded than a piston flow.

### 2.3.3. Reflect of gross maldistribution by RTD

When it comes to the case of improper distributor or collector design, the RTD curve can also be influenced by gross maldistribution. Flowrate in each pipe is imposed by a preset value according to uniform or non-uniform distribution case, as shown in Fig. 7. Such parabolic distribution shape may be observed in typical Z-type ladder networks having one inlet pipe and one outlet pipe in diagonal position and perpendicular parallel pipes [43]. The total volumetric flowrate is kept at 60 mL/min, the same value as in Sections 2.3.1 and 2.3.2.

As shown in Fig. 7(a) and (b), RTD curves under a flowrate deviation condition can differ from those under uniform distribution condition. The difference can be slight (for the case of 10% deviated flowrate, (a) but becomes very distinctive when the flowrate deviation  $Q_{dv}$  increases (b).

For channels with high flowrate (at two sides as shown in the

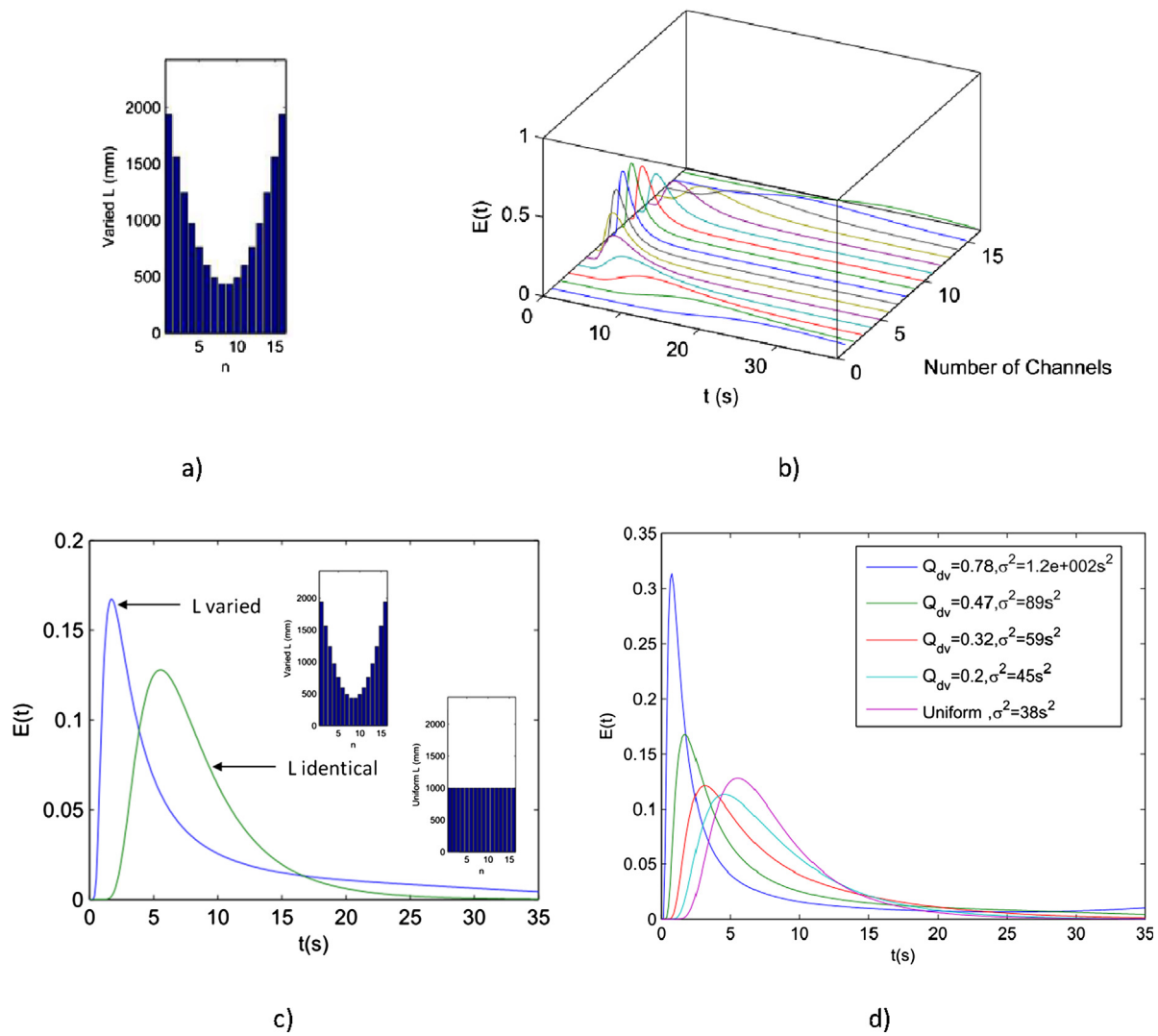


Fig. 5. Global and individual RTD curves for length varied non-uniform distribution cases.

figures), tracer peaks appear much earlier than other channels, indicating shorter average residence time. Moreover, if we examine the spreading character of the RTD curves, we find that uniform distribution curve is less stretched compared with that with fluid deviation.  $Pe$  number in these channels is higher and flow is closer to plug flow.

The influence of maldistribution on RTD depends highly on flowrates. At low flowrate, the influences are easier to be distinguished compared with high flowrates. In other words, the distribution issue at low flowrate has more influence on the global RTD curve and may result in more serious performance deterioration.

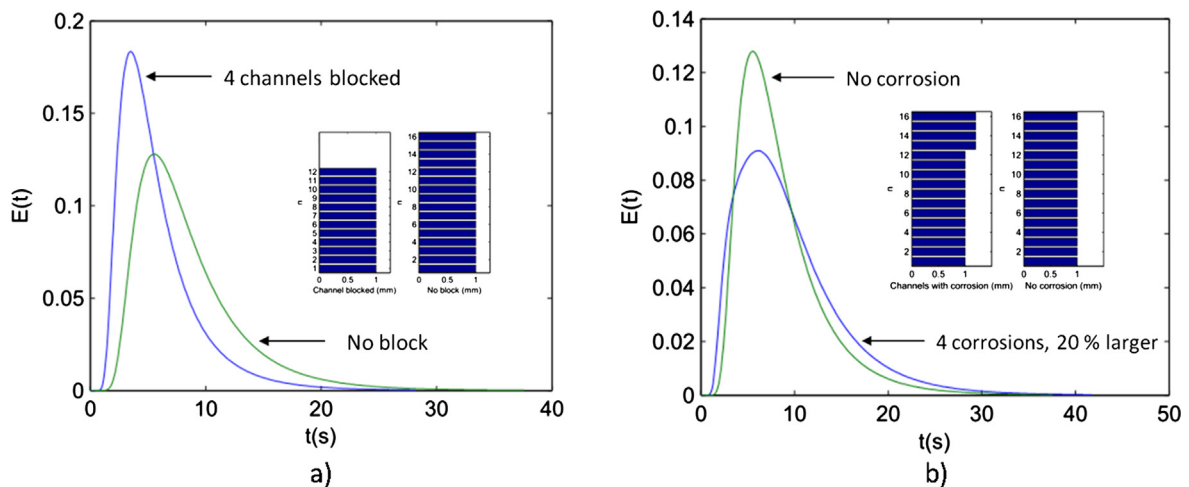


Fig. 6. Global RTD curves for block (a) and corrosion (b) cases.

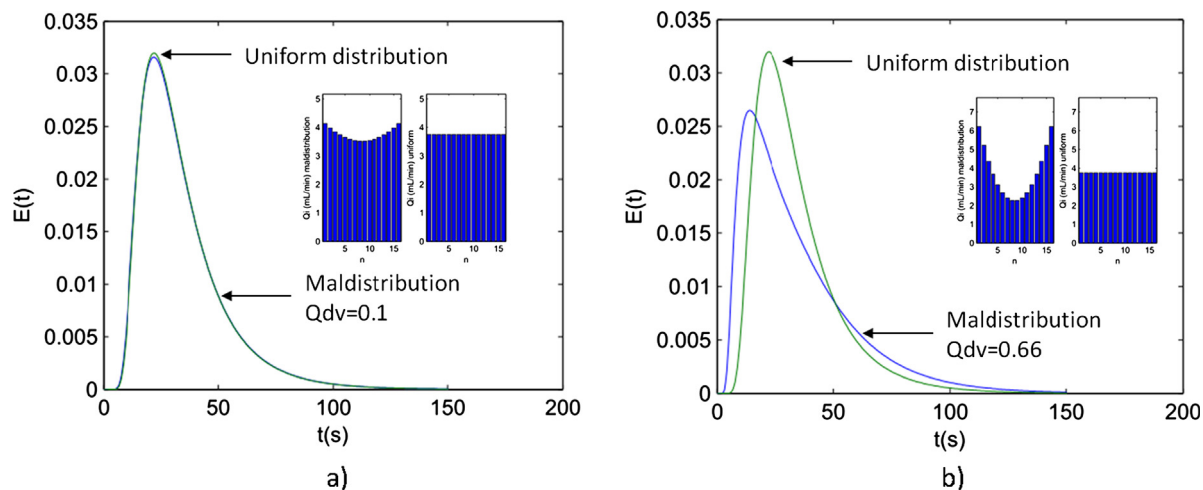


Fig. 7. Global RTD curves for gross maldistribution.

#### 2.3.4. Discussion

Other case studies were also performed, covering different channel numbers, different total flowrates or different  $Q_{dv}$  variations. Although the shapes of global RTD curves and the corresponding  $\sigma^2$  values may vary case by case, the general trend is similar as the cases presented above. A global RTD curve appearing stretched or distorted (longer tailing, multiple peaks, etc.) with higher  $\sigma^2$  value usually implies the presence of uneven flow distribution.

In all cases of non-uniform distribution, the inhomogeneity of residence time may degrade the global performance. For example as shown in Fig. 5, peak concentration in the varied length case arrives at 2.5 s instead of 6.5 s for identical length case. This information can be obtained by RTD tests and thus shows as an effective internal flow identification tool. Regarding heat transfer, local heat transfer coefficient depends on individual channel velocity (flowrate). The above RTD modelling results show how important a uniform fluid distribution should be kept in multichannel devices. The use of some optimised structures such as tree-like distributor [10], flat constructal distributor/collector [7,17], etc., may help providing even fluid distribution to avoid the above issue.

The analyses of the three maldistribution cases confirm the feasibility of reflecting fluid distribution characters by RTD test, instead of currently used visualisation or numerical methods. The next part focuses on the development and implementation of a tracer test platform on multichannel devices.

### 3. High-speed RTD measurement

#### 3.1. RTD detection system

The high-speed tracer test platform is comprised of a high-speed camera, two lab-devised miniflowcells for ink observation, and an HPLC valve for tracer injection. Sampling time of this platform, which is critical for a short impulse response measurement, could be as short as 1 ms (1000 Hz) according to the frame-rates of the fast camera.

The test platform is described in Fig. 8. One gear pump is used to circulate fluid through the 16-channel device. Here the device has two inlets and one outlet since it is initially designed to be multifunctional serving as both fluid mixers, heat exchangers and reactors. Details about the configuration can be found in our previous papers [10,15]. More specifically, the equal fluid distribution is confirmed being under 10% among the 16 channels. Tracer is injected to one of the inlets of device through using an HPLC valve, which is usually used for rapid injection of a fixed volume of liquid. The other inlet was blocked during the RTD measurement. By doing this, both the fluid distribution,

collection and multichannel parts are investigated by RTD. Two miniflowcells are placed shortly before the inlet and after the outlet of the multichannel device. The distance is kept as short as possible to avoid possible influence on the result. LED sources are employed to provide sufficient and adjustable luminance to the miniflowcells. Synchronised fast cameras are used to capture photos during the testing process. Water serves as the main circulation fluid through the multichannel device.

Carbon ink is chosen as the tracer in this test. Particles of carbon with sizes around 1  $\mu\text{m}$  are dispersed homogeneously in water. By diluting the inks into water in a trial-and-error manner, we realise an inverted grey scale change varying from 255 (white, no tracer detected) to the zero (black, most concentrated). In our case, we use an 8-bit image scale corresponding to a maximum grey scale of 255. Advantages of using inks are: (i) chemically stable; (ii) easy to be detected with monochrome fast camera; (iii) non-adhesive to pipe wall; (iv) environment harmless; (v) negligible influence on the physical properties of liquid; etc.

As the key detection unit of this tracer test, two miniflowcells are designed and fabricated (Fig. 9) in laboratory. Basically, the miniflowcell provides a narrow flow path of 0.5 mm for fluid so that light passed through the miniflowcell is inversely proportional to the concentration of tracer. Photo sequences taken by fast camera every 1 ms then reflect different grey scales. Through image analyses and data normalisation, evolution of the tracer concentration with time is obtained.

As it is practically impossible to realise a real Dirac injection, short pulse input is generally used. For all test cases, the injection tracer volume is fixed at 15  $\mu\text{L}$  by the HPLC 6-way valve.

#### 3.2. Signal treatment

Image treatment and post analyses are implemented using an open source tool ImageJ [44]. Grey scales of captured image sequences with time stamp are analysed in a 'Batch' manner, i.e. a large quantity of time-labelled photos are analysed in a single process. Concentration of tracers is then calculated with respect to time. Finally, inlet and outlet concentration curves are normalised so that the surface area under the curves equals 1.

Several precautions should be taken before and during the experiments. First of all, the injection of tracers should be done after agitating the tracer solutions. Ink particles tend to agglomerate after being left still for several hours. The appearance of ink particle agglomerations (shown in Fig. 10b) may influence the continuity of measurement, thus the accuracy on the concentration. Special attention should be given



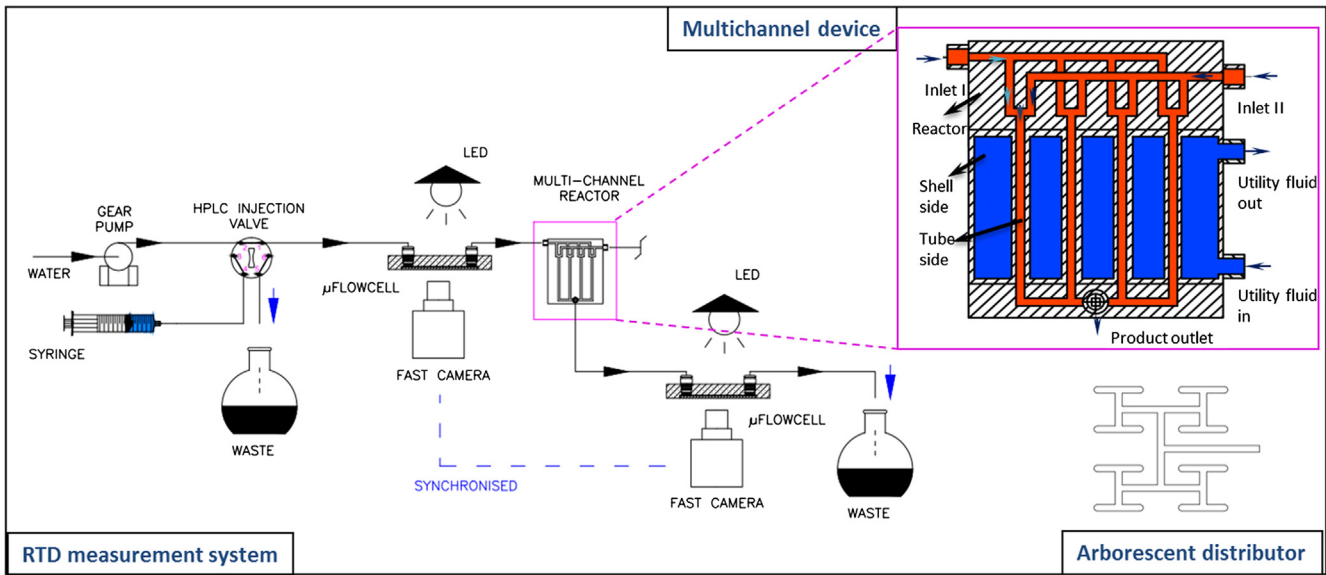


Fig. 8. A tracer test platform and its working principle for a rapid residence time distribution characterisation of a multichannel device.

during the injection progress. Some air bubbles may enter the system when injecting the small volume of tracer by HPLC valve. This may also give noise to the measuring results (see Fig. 10c) and should be avoided. One way to prevent air from passing inside is to switch the valve in a very fast manner. Some researchers used electric solenoid or piezoelectric actuator to switch the valve as presented in the paper [45].

### 3.3. Post processing

#### 3.3.1. Beer-Lambert law

The relationship between ink concentration and captured light intensity is exponential according to Beer-Lambert law:

$$I = I_0 e^{-\varepsilon_{ink} l C} \tag{11}$$

where  $I$  stands for the light intensity measured after the miniflowcell with ink-in-water as medium, and  $I_0$  is that with pure water as medium;  $\varepsilon_{ink}$  is the extinction coefficient of ink,  $L \cdot mol^{-1} \cdot cm^{-1}$ ;  $l$  the optical path of miniflowcell, cm; and  $C$  the concentration of ink in water,  $mol \cdot L^{-1}$ .

With  $\varepsilon_{ink}$  and  $l$  being constants, an exponential relationship between concentration and light intensity can relate images grey scale with concentration:

$$C \propto \ln \frac{I_0}{I} = \ln \frac{G_0}{G} \tag{12}$$

where  $G$  is the inversed grey scale of images, 0 to 255;  $G_0 = 255$  is the inversed grey scale value in the case of pure water. It worth noting that

the minimum value of measured  $G$  in our experiment is kept higher than 0, i.e., the darkest image is not fully opaque. This is to guarantee that even in case of the highest concentration, the grey scale is still under saturated.

Obtained concentration  $C$  should still be normalised so that the area under the concentration/time curve equals 1.

#### 3.3.2. Noise elimination

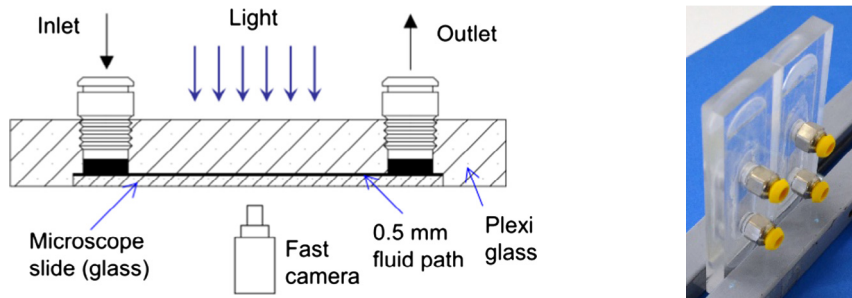
Random noises could be eliminated by applying higher frequency noise removal. The simplest method is the moving average one, suitable for large deviated noise eliminating. Preset value of noise limit is obtained by trial-and-error.

$$\begin{aligned} & \text{if } C(n+1) - C(n) > \text{set\_value} \\ & C(n+1) = (C(n-1) + C(n))/2 \end{aligned} \tag{13}$$

#### 3.3.3. RTD model fitting

Two theoretical RTD models may be used to approximately represent the flow behaviour in the multichannel device: DPF model (Eq. (1)) and compartment model [31,37]. The later combines a PF portion and a fully mixed one (CSTR), by defining a volumetric plug flow proportion  $\theta_p$ .

The compartment model considers part of the reactor volume being PF (P) and the other part being CSTR (M) and it can be expressed by:



a) concept of the lab-developed miniflowcell      b) photo of the two miniflowcells

Fig. 9. Miniflowcell design for rapid RTD detection.

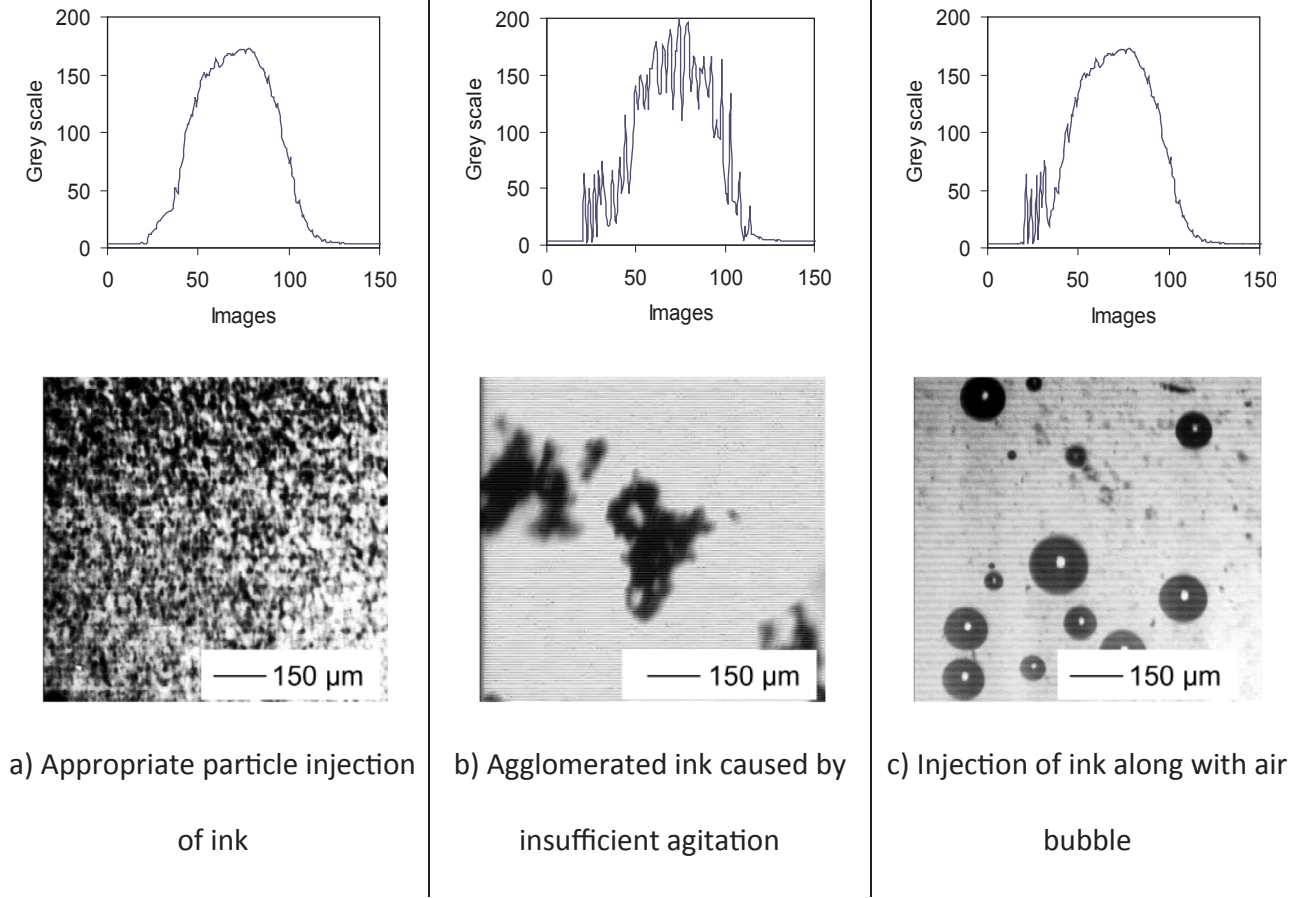


**Fig. 10.** Ink injection should be prepared with precaution and cases should be avoided like (b) agglomeration and (c) bubble presence; Obtained grey scale curves are shown above the images (Images captured through fast camera and miniflowcells, post processed through ImageJ).

$$E(\theta) = \begin{cases} 0 & \text{for } \theta < \theta_p \\ \frac{1}{1-\theta_p} \exp\left(\frac{\theta_p}{1-\theta_p} - \frac{\theta}{1-\theta_p}\right) & \text{for } \theta \geq \theta_p \end{cases} \quad (14)$$

where  $\theta = t/\tau_m$  is the dimensionless time,  $\theta_p = \tau_p/\tau_m$ ,  $\tau_m = \tau_p + \tau_M$  and  $\tau_p/\tau_M = V_p/V_M$ , RTD  $E(t)$  of this model can be calculated with known mean residence time  $\tau_m$  and given  $\theta_p$ .

To approximately fit the measured response curve with one of the two theoretical RTD models, basic parameters are firstly pre-set. It concerns the  $Pe$  number for the case of DPF and plug flow volume proportion  $\theta_p$  for compartment PF-CSTR model. Then, RTD models are obtained by using spatial pass-through time ( $\tau_{m,spatial}$ ) as the mean residence time. Next, RTD models are convoluted with experimental input signal to simulate a standard model response to the real injection. The difference between convoluted model response and tested response is minimized by adjusting  $Pe$  or  $\theta_p$  by an iterative calculation.

Calculation of outlet concentration from inlet tracer concentration and  $E(t)$  is a forward problem and it involves a convolution process according to Eq. (15). Convolution tool of Matlab© is utilized for this procedure.

$$C_{out}(t) = \int_0^t C_{in}(t-t') \cdot E(t') dt' \quad (15)$$

Model predicted RTD is obtained by adjusting different parameters ( $Pe$  for DPF model and  $\theta_p$  for PF + CSTR model). In this step, the cumulative deviation between convoluted response  $C_{out,fit}$  and measured response  $C_{out,test}$  is integrated:

$$E_{fit} = \int_0^\infty |C_{out,fit}(t_i) - C_{out,test}(t_i)| dt = \sum_{i=1}^n |C_{out,fit}(t_i) - C_{out,test}(t_i)| \Delta t \quad (16)$$

During the fitting process, the  $E_{fit}$  is minimized to identify the most appropriate  $Pe$  and  $\theta_p$  values. The defined cumulative error has a maximum value of 1 since both  $C_{in}$  and  $C_{out}$  signals are normalized. The smaller this value, the closer the model convoluted response from measured response. Corresponding RTD expressions are then obtained.

### 3.3.4. Determination of mean residence time

The first calculation of mean residence time is through the spatial circulating time of fluid through studied volume:

$$\tau_{m,spatial} = V/Q \quad (17)$$

The other way of mean residence time determination is from the basics of RTD. After tracer tests, the mean residence time could be calculated by the difference between the average injection time and outlet time, subtracted by the time passing through the detecting miniflowcell:

$$\tau_{m,measured} = \tau_{response} - \tau_{inject} - \tau_{flowcell} = \frac{\sum_{i=1}^n t_i C_{out}(t_i)}{\sum_{i=1}^n C_{out}(t_i)} - \frac{\sum_{i=1}^n t_i C_{in}(t_i)}{\sum_{i=1}^n C_{in}(t_i)} - V_{flowcell}/Q \quad (18)$$

The comparison of the two residence times helps verify the precision level of the measurement tool.

**Table 1**  
Summary of five RTD tests and their corresponding conditions.

Test	Flowrate $Q$ ( $\text{mL min}^{-1}$ )	Maximum $Re$ (–)	Channel $Re$ (–)	Theoretical pass-through time $\tau_m$ (s)
R1	280	2324	185	1.05
R2	325	2698	215	0.91
R3	400	3320	264	0.74
R4	440	3652	291	0.67
R5	493	4094	326	0.6

### 3.4. Results and discussions

A series of five tests is implemented to the 16-channel device. Tests are carried out under stable state without any leakage or tracer absorbance. Several flowrate conditions are tested and their characteristic parameters including  $Re$  and spatial pass through time are shown in Table 1.

Regarding the flow regime, it worth noting that the tested reactor is a multichannel device with arborescent (tree-like) distributor and collector. Flowrates in different levels of the multi-scale structure differ so as to the corresponding  $Re$  number. For example in the case of R1, a total flowrate of  $280 \text{ mL}\cdot\text{min}^{-1}$  gives a maximum  $Re$  of 2324 (transitional flow in the collector outlet), while that of channel  $Re$  is 185 (laminar). Therefore, different flow regimes co-exist in this multichannel device, with channel flow basically being laminar.

#### 3.4.1. Tracer concentration curves

Curves of Injection and response in tested cases are shown in Fig. 11. Under different flowrate conditions, the injection and response concentration curves are clearly distinguished. As in the lowest flowrate case, i.e. R1, both inlet and outlet concentration curves last longer than the other tests. The expanded concentration is mainly due to the low volume flowrate imposed to R1. From R1 to R5, the inlet and outlet concentration durations decrease with flowrate augmentation.

The output concentration is more expanded than its corresponding input one, showing a dispersive character due to the internal multichannel structure. For each of the five cases, the tracer is detected during longer time than its corresponding input signal. As the case of R5, its injected tracers become undetected starting from 0.6 s. On the other hand, the output tracers are observed starting from 1.1 s and disappear from the detection miniflowcell at 2.2 s. The pulse interval changes from 0.6 s at the inlet to 1.1 s at the outlet, meaning a significant dispersive mixing inside the heat exchanger reactor.

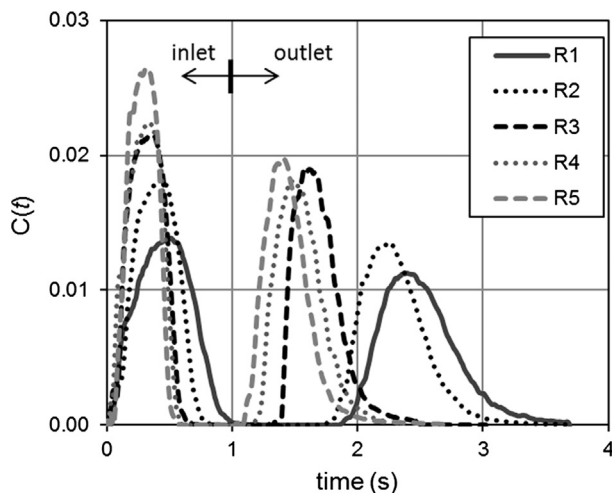


**Fig. 11.** Experimental RTD input and response through multichannel device, cases from R1 to R5, total flowrate increased from  $280 \text{ mL}\cdot\text{min}^{-1}$  (R1) to  $493 \text{ mL}\cdot\text{min}^{-1}$  (R5).

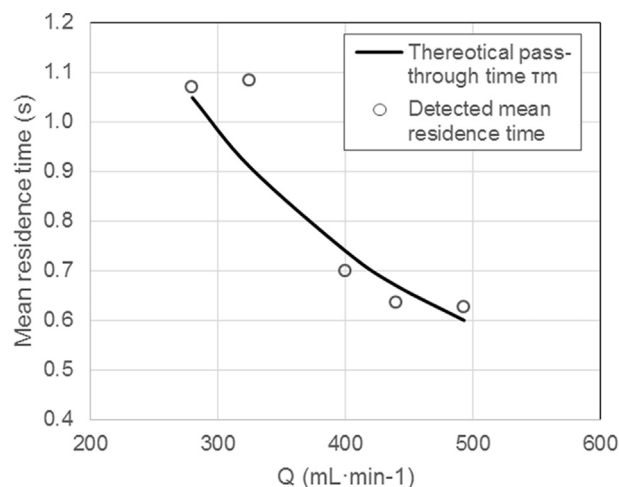


**Fig. 12.** Comparison on theoretical pass-through time and detected mean residence time, cases from R1 to R5, indicating an average error of 7.2%.

#### 3.4.2. Precision verification by mean residence time

To examine the precision of the tracer test process, the measured residence time and the theoretical spatial pass-through time are plotted in Fig. 12. Both residence times follow an inversely proportional character with flowrate. In most cases, the two residence times are close to each other, except for that of the case R2 ( $325 \text{ mL}\cdot\text{min}^{-1}$ ). The average relative error is 7.2% and that of maximal error is 19.1% (case of R2). The reasons for uncertainties are twofold. First, instrumentation errors exist in flowrate determination and tracer concentration detection. For example, the significantly deviated case R2, observed after repeated tests, is probably due to mechanical vibration resonance between the pump and the tested device. Second and most probably, the complex flow characteristic of the studied device, including distribution/16-channel/collection zones and each of them has different flow regimes, may give uncertainties. This will be discussed in the model fitting part.

#### 3.4.3. Model fitting results

Theoretical fitted DPF and PF-CSTR RTD  $E(t)$  and  $E(\theta)$  curves are shown in Figs. 13 and 14, along with identified  $Pe$  and  $\theta_p$  values. Fitting errors between experimental results and both models range from 10% to 22%, with the PF-CSTR model closer to the experimental results. These curves eliminate the imperfect impulse injection effect on the response, and they provide information such as residence time, plug flow degree, mixing volume fraction, etc.

First of all, as discussed earlier, the residence time shortens with increasing flowrate. For higher flowrates, the first detection of tracer arrives earlier and this can be observed both from the DPF fitted result and the PF-CSTR one.

Secondly, from the DPF results, the plug flow degree for all cases are very high with an identified value of  $Pe$  ranging from 168 (R5) to 317 (R3). In general, a  $Pe$  number higher than 100 is considered as a highly plug flow. This plug flow seems to be more distinguished for the case R3, with a  $Pe$  number of 317.

Finally, examining the parameter  $\theta_p$  may give information on the proportion of mixing volume in the total volume. As the compartment model separates the reactor in two parts: a part of perfect mixing and the other perfect plug flow, it may be more adapted to our system including tree-like distributor/collector and 16 channels. Experimental  $\theta_p$  ranges between 0.87 (R5) and 0.91 (R3), indicating around 90% of the total volume being occupied by pure plug flow. Thus, only a small portion of volume in the reactor is used as mixing volume and in particular in the tree-like split-and-combine structure.

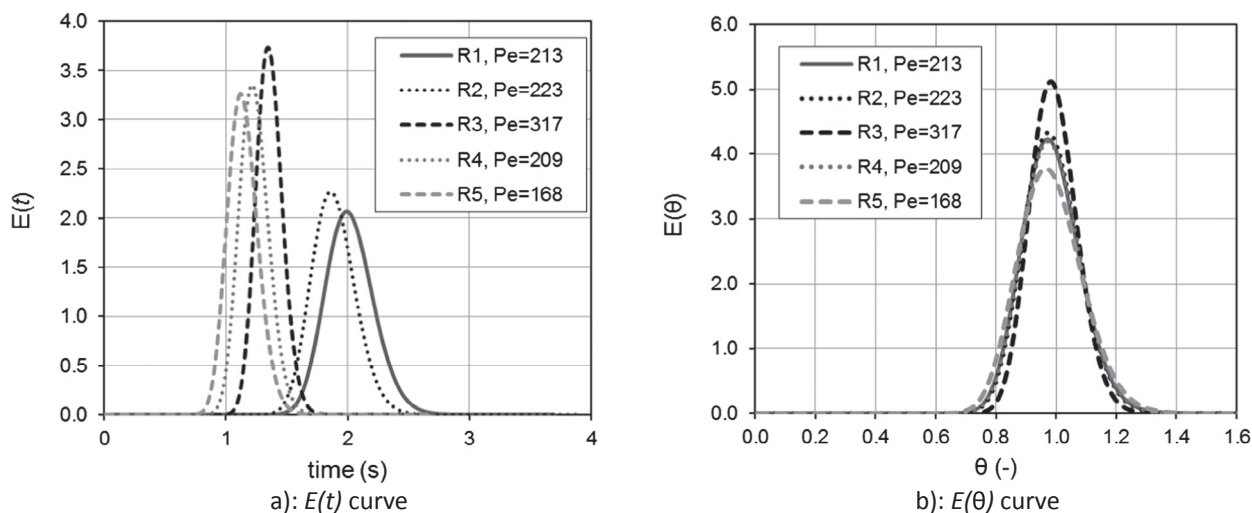


Fig. 13. RTD curves obtained by DPF model fitting.

3.4.4. Discussion

The first conclusion by examining the RTD curves of the multi-channel device is on the fluid distribution uniformity. As discussed earlier in this paper, flowrate deviation among channels may give rise to distorted RTD curves such as higher variance, double peak in the response curve, etc. Since none of our test results (R1-R5) reflects a second peak, fluid distribution is thus considered to be relatively uniform.

According to a correlation given by Levenspiel [31], for a DPF flow and with  $Pe$  higher than 1, the RTD curve variance is inversely proportional to  $Pe$  by:

$$\sigma_{\theta}^2 = \frac{2}{Pe} \tag{19}$$

Fig. 15 demonstrates the comparison between the theoretically and experimentally obtained relationship between  $Pe$  number and normalized variance. From the figure, the test result is shown to hold the same trend as that given by theory. The difference in value is mainly due to the fitting deviation from original signal to model convolution. This comparison can also serve as a verification of the effectiveness of the developed RTD measuring system.

Earlier study [10] on the same multichannel device has revealed efficient mixing effect, both in macro scale and micro scale. It may be interesting to compare the low volume used for mixing from the RTD

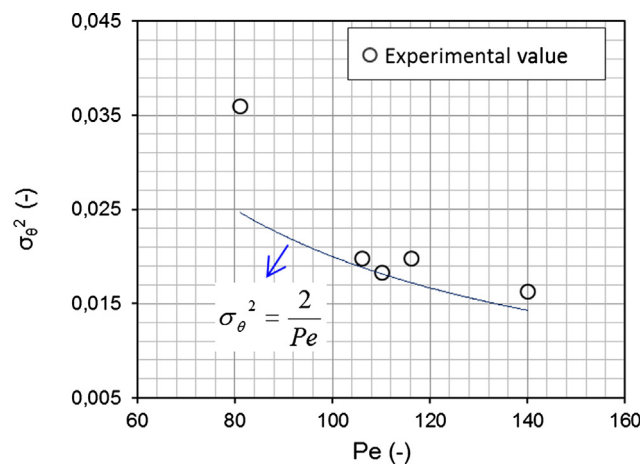


Fig. 15. RTD normalized variance with respect to Peclet number (DPF model fitting).

tests. As discussed earlier, only 10% of the total volume has been used for species mixing. As a result, the mixing effect happens in a very local position in the reactor. The rest of the device, however, is characterised by highly plug flow.

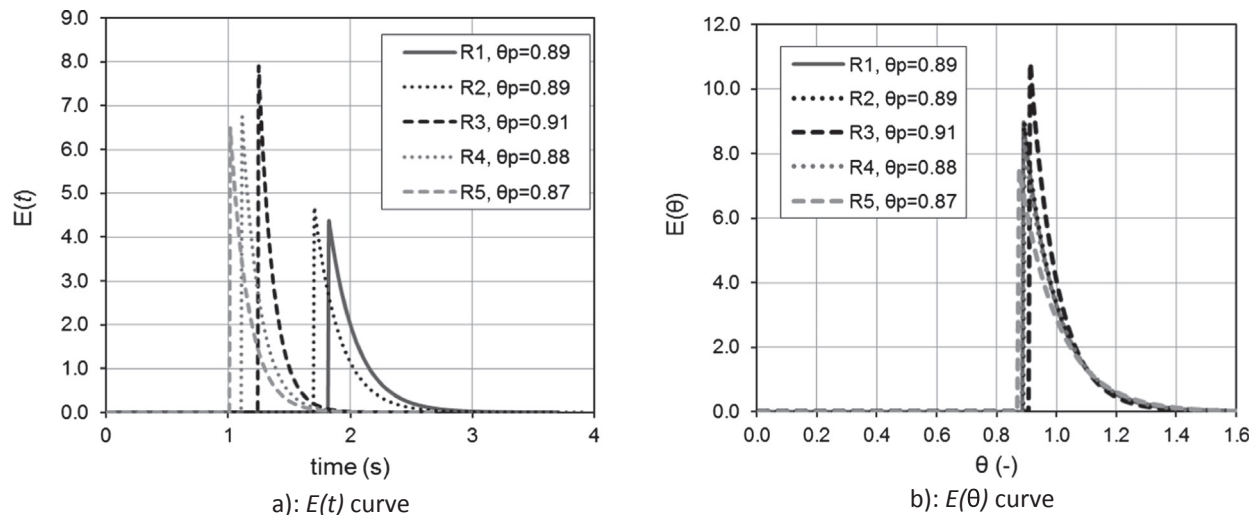


Fig. 14. RTD curves obtained by PF-CSTR model fitting.

For such a multichannel complex flow system as studied, being high degree plug flow does not conflict with its efficient mixing character. On the contrary, a reactor with very local and efficient mixing, while with plug flow for the reaction functional part, is beneficial for undertaking chemical reactions. If comparing with a CSTR reactor, the advantage of current reactor is the local mixing effect instead of mixing in the global reactor size.

Finally, both DPF and PF-CSTR models can be implemented for the model fitting and they give different information and precisions. The currently tested 16-channel system represents a relative short pipe flow ( $L/d = 50/2$  cm), connected to a distributor and a collector. This configuration is more adapted to PF-CSTR model since it separates the volume into two zones. In the case of higher length/diameter ratios and without distributor/collector (e.g., the cases in the modelling part), the DPF model might be more adapted for the fitting process.

#### 4. Conclusions

A RTD model for multichannel devices, considering diameter, length and distributor/collector induced flowrate variations is constructed in this study. Different situations are analysed using the model and compared with that of perfectly uniform distribution situation.

Comparisons show how fluid distribution uniformity may be reflected by global RTD curve. For example, compared with the case of even length distribution, a varied-length system will receive its peak concentration earlier, meaning a shorter fluid passage time for some channels. However, its tail could last much longer than that of uniform length case. Similar results can be obtained for the cases of channel blockage, corrosion, and gross maldistribution (due to distributor design).

These results demonstrate that RTD can be a useful tool for the diagnostic of flow distribution non-uniformity. The identification of the above-mentioned problems in multichannel devices using non-intrusive tracer test is then possible.

An experimental platform is then constructed taking a 16-channel device as example. The ink-based tracer test platform, together with fast camera detection, is able to determine narrow RTD with mean residence time as short as 600 ms. The RTD test shows a uniform flowrate distribution and quasi plug flow pattern ( $Pe > 168$ ) in the tested multichannel device with no short-circuit, back flow or stagnant area observed. Together with its data processing procedure, the experiment platform can be used to characterize various millimetric multichannel devices with short or long pass-through time.

Our future efforts are emphasized on applying the above theoretical and experimental approaches to other type of multi-channel systems, with a special attention on the fluid distribution issue according to distributor design.

#### References

- [1] A. Stankiewicz, J.A. Moulijn, Process intensification: transforming chemical engineering, *Chem. Eng. Prog.* 96 (2000) 22–34.
- [2] T. Van Gerven, A. Stankiewicz, Structure, energy, synergy, time-the fundamentals of process intensification, *Ind. Eng. Chem. Res.* 48 (2009) 2465–2474, <https://doi.org/10.1021/ie801501y>.
- [3] M. Wei, Y. Fan, L. Luo, G. Flamant, Fluid flow distribution optimization for minimizing the peak temperature of a tubular solar receiver, *Energy* 91 (2015) 663–677, <https://doi.org/10.1016/j.energy.2015.08.072>.
- [4] M.N. Kashid, A. Gupta, A. Renken, L. Kiwi-Minsker, Numbering-up and mass transfer studies of liquid-liquid two-phase microstructured reactors, *Chem. Eng. J.* 158 (2010) 233–240.
- [5] M. Saber, J.M. Commenge, L. Falk, Microreactor numbering-up in multi-scale networks for industrial-scale applications: impact of flow maldistribution on the reactor performances, *Chem. Eng. Sci.* 65 (2010) 372–379.
- [6] O. Tomomura, T. Tominari, M. Kano, S. Hasebe, Operation policy for micro chemical plants with external numbering-up structure, *Chem. Eng. J.* 135 (2007) S131–S137, <https://doi.org/10.1016/j.cej.2007.07.006>.
- [7] J. Yue, R. Boichot, L. Luo, Y. Gonthier, G. Chen, Q. Yuan, Flow distribution and mass transfer in a parallel microchannel contactor integrated with constructal distributors, *AIChE J.* 56 (2010) 298–317, <https://doi.org/10.1002/aic.11991>.
- [8] D. Tarlet, Y. Fan, S. Roux, L. Luo, Entropy generation analysis of a mini heat exchanger for heat transfer intensification, *Exp. Therm. Fluid Sci.* 53 (2014) 119–126, <https://doi.org/10.1016/j.expthermflusc.2013.11.016>.
- [9] Y. Fan, R. Boichot, T. Goldin, L. Luo, Flow distribution property of the constructal distributor and heat transfer intensification in a mini heat exchanger, *AIChE J.* 54 (2008) 2796–2808.
- [10] X. Guo, Y. Fan, L. Luo, Mixing performance assessment of a multi-channel mini heat exchanger reactor with arborescent distributor and collector, *Chem. Eng. J.* 227 (2013) 116–127, <https://doi.org/10.1016/j.cej.2012.08.068>.
- [11] P. Zhou, D. Tarlet, M. Wei, Y. Fan, L. Luo, Novel multi-scale parallel mini-channel contactor for monodisperse water-in-oil emulsification, *Chem. Eng. Res. Des.* 121 (2017) 233–244, <https://doi.org/10.1016/j.cherd.2017.03.010>.
- [12] Z. Fan, X. Zhou, L. Luo, W. Yuan, Evaluation of the performance of a constructal mixer with the iodide-iodate reaction system, *Chem. Eng. Process. Process Intensif.* 49 (2010) 628–632, <https://doi.org/10.1016/j.cep.2010.04.005>.
- [13] J.M. Commenge, L. Falk, J.P. Corriou, M. Matlosz, Analysis of microstructured reactor characteristics for process miniaturization and intensification, *Chem. Eng. Technol.* 28 (2005) 446–458, <https://doi.org/10.1002/ceat.200500017>.
- [14] L. Falk, J.M. Commenge, Performance comparison of micromixers, *Chem. Eng. Sci.* 65 (2010) 405–411.
- [15] X. Guo, Y. Fan, L. Luo, Multi-channel heat exchanger-reactor using arborescent distributors: a characterization study of fluid distribution, heat exchange performance and exothermic reaction, *Energy* 69 (2014) 728–741, <https://doi.org/10.1016/j.energy.2014.03.069>.
- [16] X. Guo, Intensification des transferts dans un mini-échangeur multicanaux multi-fonctionnels, Université de Grenoble, 2013.
- [17] Y. Su, G. Chen, E.Y. Kenig, An experimental study on the numbering-up of microchannels for liquid mixing, *Lab Chip* 15 (2015) 179–187, <https://doi.org/10.1039/C4LC00987H>.
- [18] H. Liu, P. Li, J.V. Lew, CFD study on flow distribution uniformity in fuel distributors having multiple structural bifurcations of flow channels, *Int. J. Hydrogen Energy.* 35 (2010) 13.
- [19] J. Aubin, M. Ferrando, V. Jiricny, Current methods for characterizing mixing and flow in microchannels, *Chem. Eng. Sci.* 65 (2010) 2065–2093, <https://doi.org/10.1016/j.ces.2009.12.001>.
- [20] C. Pistoiesi, Y. Fan, L. Luo, Numerical study on the improvement of flow distribution uniformity among parallel mini-channels, *Chem. Eng. Process. Process Intensif.* 95 (2017) 63–71.
- [21] M. Wei, Y. Fan, L. Luo, G. Flamant, CFD-based evolutionary algorithm for the realization of target fluid flow distribution among parallel channels, *Chem. Eng. Res. Des.* 100 (2015) 341–352, <https://doi.org/10.1016/j.cherd.2015.05.031>.
- [22] S. Panić, S. Loebecke, T. Tuercke, J. Antes, D. Bošković, Experimental approaches to a better understanding of mixing performance of microfluidic devices, *Chem. Eng. J.* 101 (2004) 409–419.
- [23] A.D. Stroock, S.K. Dertinger, G.M. Whitesides, A. Ajdari, Patterning flows using grooved surfaces, *Anal. Chem.* 74 (2002) 5306–5312.
- [24] A.D. Stroock, S.K.W. Dertinger, A. Ajdari, I. Mezic, H.A. Stone, G.M. Whitesides, Chaotic mixer for microchannels, *Science* 80 (295) (2002) 647–651.
- [25] G. Boutin, M. Wei, Y. Fan, L. Luo, Experimental measurement of flow distribution in a parallel mini-channel fluidic network using PIV technique, *Asia Pacific J. Chem. Eng.* 11 (2016) 630–641.
- [26] M. Wei, G. Boutin, Y. Fan, L. Luo, Numerical and experimental investigation on the realization of target flow distribution among parallel mini-channels, *Chem. Eng. Res. Des.* 113 (2016) 74–84, <https://doi.org/10.1016/j.cherd.2016.06.026>.
- [27] F. Huchet, J. Comiti, P. Legentilhomme, C. Sollic, J. Legrand, A. Montillet, Multi-scale analysis of hydrodynamics inside a network of crossing minichannels using electrodiffusion method and PIV measurements, *Int. J. Heat Fluid Flow.* 29 (2008) 1411–1421, <https://doi.org/10.1016/j.ijheatfluidflow.2008.04.012>.
- [28] O. Pust, T. Strand, P. Mathys, A. Rütli, Quantification of laminar mixing performance using Laser-Induced Fluorescence, 2006.
- [29] R.B. MacMullin, M. Weber, The theory of short-circuiting in continuous flow mixing vessels in series and the kinetics of chemical reactions in such systems, *Trans. Am. Inst. Chem. Eng.* 31 (1935) 409–458.
- [30] P.V. Danckwerts, Continuous flow systems. Distribution of residence times, *Chem. Eng. Sci.* 2 (1953) 1–13.
- [31] O. Levenspiel, *Chemical Reaction Engineering*, third ed., Wiley, New York, 1999.
- [32] S. Fogler, *Essentials of Chemical Reaction Engineering*, first ed., Pearson Education Inc, Boston, 2011.
- [33] S. Klutz, S.K. Kurt, M. Lobedann, N. Kockmann, Narrow residence time distribution in tubular reactor concept for Reynolds number range of 10–100, *Chem. Eng. Res. Des.* 95 (2015) 22–33, <https://doi.org/10.1016/j.cherd.2015.01.003>.
- [34] I.V. Koptuyug, K.V. Kovtunov, E. Gerkema, L. Kiwi-Minsker, R.Z. Sagdeev, NMR microimaging of fluid flow in model string-type reactors, *Chem. Eng. Sci.* 62 (2007) 4459–4468, <https://doi.org/10.1016/j.ces.2007.04.045>.
- [35] J. Aubin, L. Prat, C. Xuereb, C. Gourdon, Chemical Engineering and Processing: process Intensification Effect of microchannel aspect ratio on residence time distributions and the axial dispersion coefficient, *Water.* 48 (2009) 554–559, <https://doi.org/10.1016/j.cep.2008.08.004>.
- [36] F. Trachsel, A. Günther, S. Khan, K.F. Jensen, Measurement of residence time distribution in microfluidic systems, *Chem. Eng. Sci.* 60 (2005) 5729–5737.
- [37] C.G.C.C. Gutierrez, E.F.T.S. Dias, J.A.W. Gut, Residence time distribution in holding tubes using generalized convection model and numerical convolution for non-ideal tracer detection, *J. Food Eng.* 98 (2010) 248–256, <https://doi.org/10.1016/j.jfoodeng.2010.01.004>.
- [38] E. Georget, J.L. Sauvageat, A. Burbidge, A. Mathys, Residence time distributions in a modular micro reaction system, *J. Food Eng.* 116 (2013) 910–919, <https://doi.org/10.1016/j.jfoodeng.2013.05.004>.

- [org/10.1016/j.jfoodeng.2013.01.041](https://doi.org/10.1016/j.jfoodeng.2013.01.041).
- [39] W. Wibel, A. Wenka, J.J. Brandner, R. Dittmeyer, Reprint of: Measuring and modeling the residence time distribution of gas flows in multichannel microreactors, *Chem. Eng. J.* 227 (2013) 203–214, <https://doi.org/10.1016/j.cej.2013.05.016>.
- [40] Z. Anxionnaz, M. Cabassud, C. Gourdon, P. Tochon, Heat exchanger/reactors (HEX reactors): concepts, technologies: State-of-the-art, *Chem. Eng. Process. Process Intensif.* 47 (2008) 2029–2050, <https://doi.org/10.1016/j.cep.2008.06.012>.
- [41] Z. Dong, S. Zhao, Y. Zhang, C. Yao, Q. Yuan, G. Chen, Mixing and residence time distribution in ultrasonic microreactors, *AIChE J.* 63 (2017) 1404–1418, <https://doi.org/10.1002/aic.15493>.
- [42] MathWorks, MATLAB, MATLAB R2012b. (2012) R2012b. 10.1201/9781420034950.
- [43] M. Saber, J.M. Commenge, L. Falk, Rapid design of channel multi-scale networks with minimum flow maldistribution, *Chem. Eng. Process. Process Intensif.* 48 (2009) 723–733.
- [44] C. Schneider, W. Rasband, K. Eliceiri, ImageJ, *Nat. Methods* 9 (2012) 671–675.
- [45] D. Boskovic, S. Loebbecke, Modelling of the residence time distribution in micro-mixers, *Chem. Eng. J.* 135 (2008) S138–S146.